A Comprehensive Multi-Method Reassessment of Stratosphere-Troposphere Exchange over the Tibetan Plateau

Study event: 18-19 October 2017

Study domain: (94-104°E, 25-32°N)

Dynamical tropopause: defined by the 3-PVU surface

Lagrangian release: 00:00 UTC on 18 October 2017, covering 60-130°E, 10-45°N, and 50-590 hPa

Air parcel grid spacing: approximately 20 km horizontally and 10 hPa vertically

Total number of air parcels: 3,623,125

Residence-time sensitivity tests: 1h, 2h, 6h, 12h, and 24 h

Ozone: four-dimensional collocation with ERA5 O_3

1 Wei’s diagnostic in isobaric coordinates (Fig. 9- Fig.10 in the original manuscript)

1.1 Interpretive framework adopted in the original manuscript

Sections 3.2-3.3 of the original manuscript adopted the 3-PVU surface as the dynamical tropopause and applied the formulation of Wei (1987) in isobaric coordinates to decompose the mass flux across the tropopause into three components: the tropopause-tendency term, the horizontal-transport term, and the vertical-transport term. In the original manuscript, stratosphere-to-troposphere transport (STT) was defined as positive. Therefore, warm colors in the original figures indicate net downward transport, whereas cool colors indicate net upward transport.

The original interpretation of Figure. 9 was that the spatial structure of the total flux from 13:00 to 18:00 UTC closely resembled that of the horizontal-transport term, suggesting that this term controlled the spatial pattern of the diagnosed flux. Meanwhile, based on the regionally averaged time series, the tropopause-tendency term was interpreted as triggering the actual downward mass transport. A downward vertical-transport component was also inferred near Yangbajing. The strongest fluxes coincided spatially with the tropopause-folding region located approximately within 25-28°N and 95-99°E.

The original manuscript further interpreted the consecutive 6-hourly flux fields on 18-19 October in Figure. 10 as exhibiting pronounced temporal variability, banded dipole patterns, and alternating small-scale positive and negative structures. These features were subsequently attributed to the evolution of tropopause folding, gravity-wave disturbances, and nonlinear wave breaking.

The spatial and temporal correspondence between the folding region and the descent of high-PV, ozone-rich air can be retained as part of the dynamical evidence chain. However, in response to your comments, and considering the concern raised by Wirth and Egger (1999) that Wei’s diagnostics may be sensitive to noise in standard meteorological datasets and to cancellation between large terms, and may even yield nonzero exchange under materially conservative conditions, I conducted additional calculations and analyses using multiple diagnostic methods.

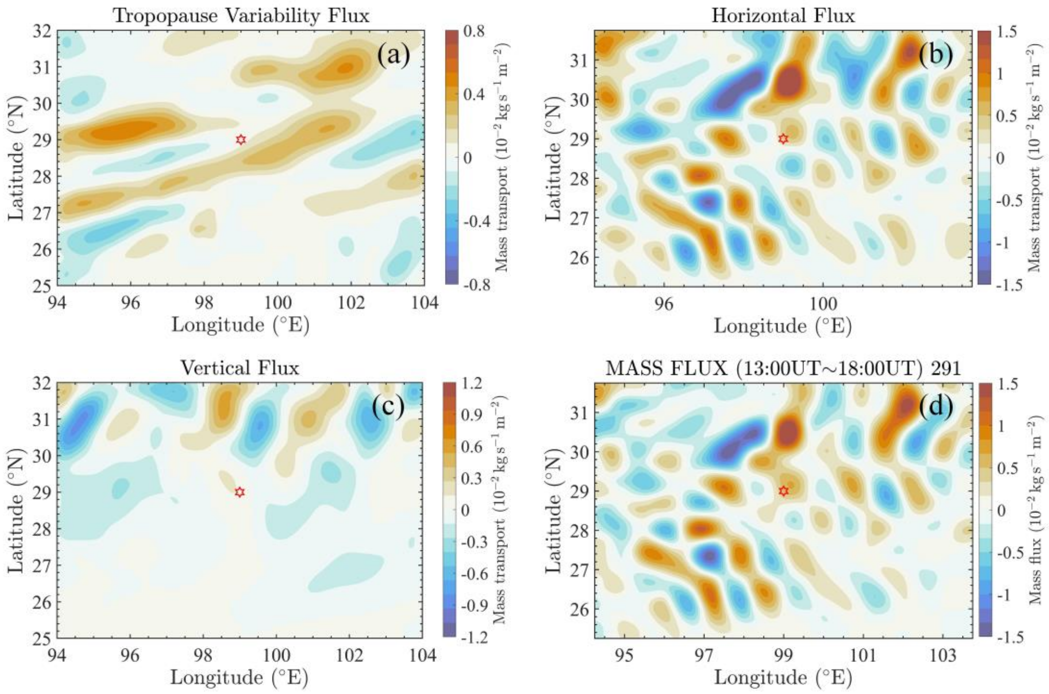

Fig.1. Figure 9 from the original manuscript: decomposition of the Wei flux in isobaric coordinates from 13:00 to 18:00 UTC. In the sign convention adopted in the original manuscript, downward STT is positive. The red star marks the Yangbajing station.

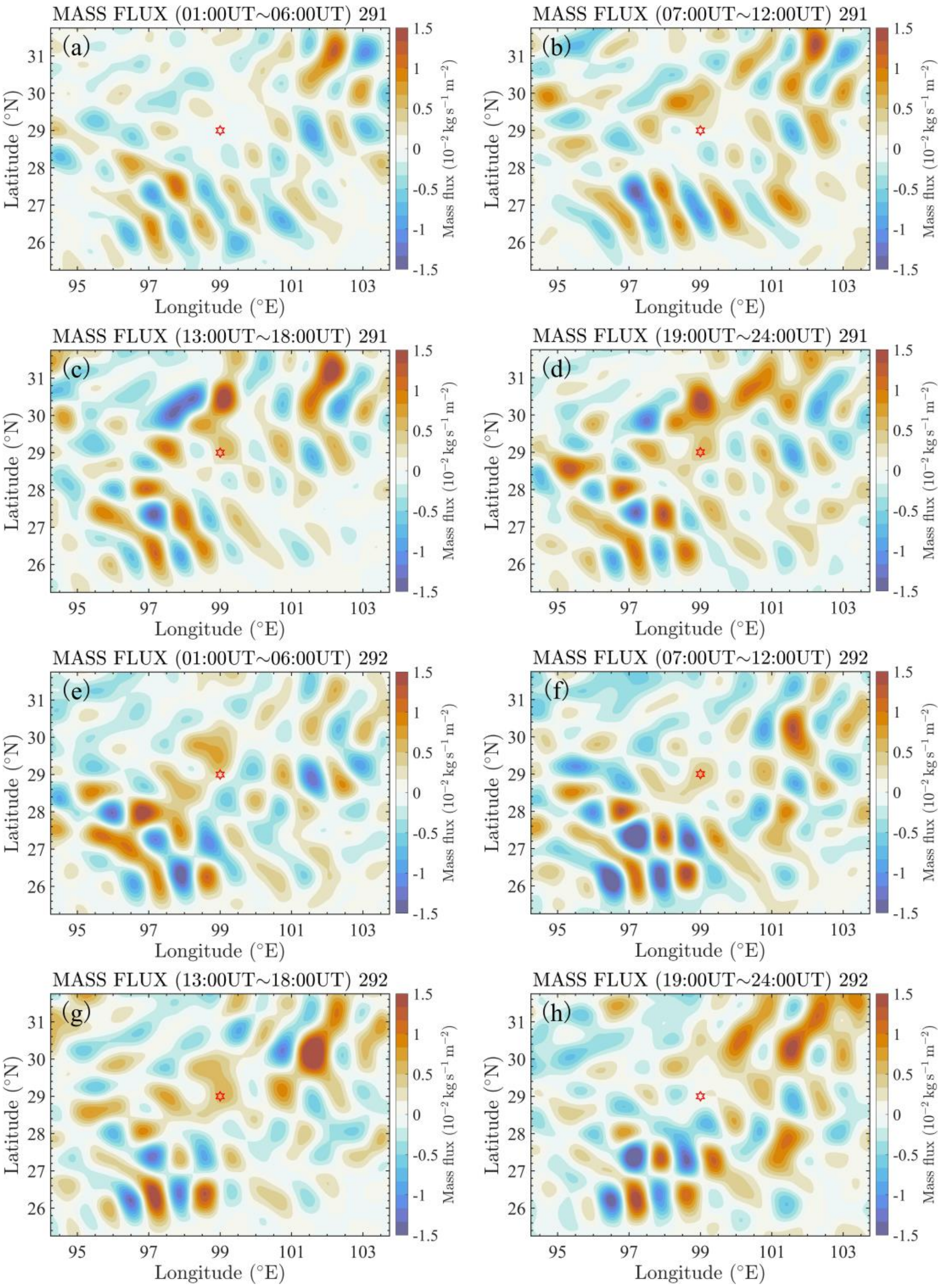

Fig.2. Figure 10 from the original manuscript: 6-hourly total Wei mass flux in isobaric coordinates during 18-19 October 2017.

2. Wei's method calculation in potential vorticity coordinates

2.1 Methods and results

To address the limitations of the Wei method in isobaric coordinates noted in your comments, and to reduce the numerical noise arising from cancellation among several large terms in that coordinate system, the Wei diagnostic was reformulated in potential vorticity coordinates. This formulation has been demonstrated to be applicable, with the dynamical tropopause defined by the 3-PVU surface. The calculation uses the three-dimensional ERA5 wind field and pressure vertical velocity to estimate the material tendency of potential vorticity along short trajectories. An equivalent Eulerian expansion is also evaluated as an internal consistency check.

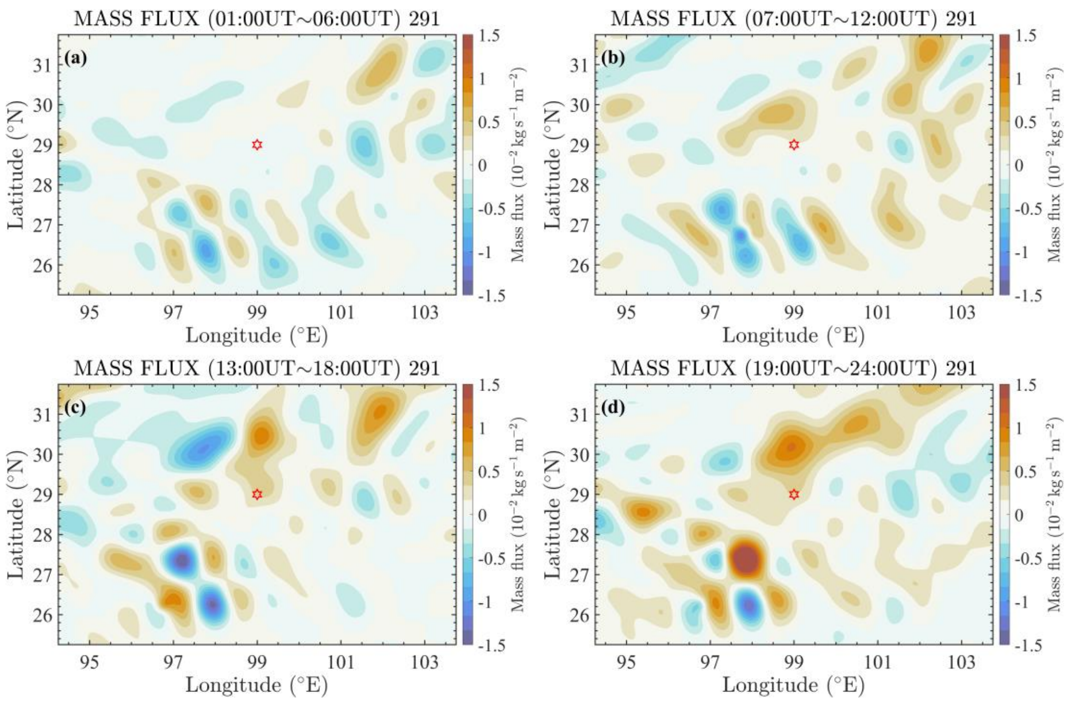

Fig.3. Wei flux in potential vorticity coordinates on 18 October 2017, averaged over 6-hour intervals.

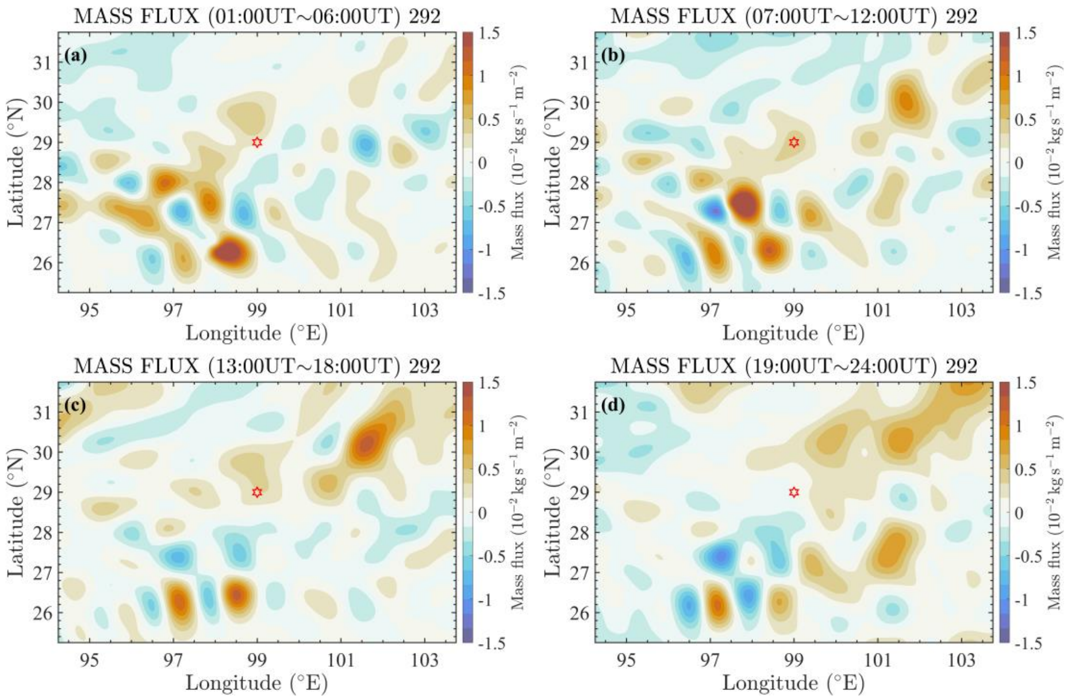

Fig.4. Wei flux in potential vorticity coordinates on 19 October 2017, averaged over 6-hour intervals.

In terms of spatial pattern, the results in potential vorticity coordinates still exhibit alternating dipole structures over 26-28°N and approximately 97-99°E. During the latter half of 18 October, these structures show some qualitative overlap with the core region identified in Fig. 10 of the original manuscript. However, the peak locations, signs, and spatial continuity do not agree on a gridpoint-by-gridpoint basis. This suggests that the coordinate transformation reduced part of the numerical noise.

3. Lagrangian method calculation

3.1 Computational design

Item	Configuration used in this study
ERA5 data	14-22 October 2017; 60-130°E, 10-45°N; 30-600 hPa
Event trajectory window	00:00 UTC on 18 October to 00:00 UTC on 20 October 2017, spanning 48 h
Air-parcel release	A single three-dimensional release over the entire source domain at 00:00 UTC on 18 October 2017
Release domain	60-130°E, 10-45°N; 50-590 hPa
Spatial resolution	Approximately 20 km in the horizontal and 10 hPa in the vertical
Total number of air parcels	3,623,125

Item	Configuration used in this study
Mass represented by each parcel	4.078865×10^{10} kg, calculated as $\Delta x^2 \Delta p/g$
Trajectory integration	Fourth-order Runge-Kutta scheme with a 15-min time step, driven by three-dimensional ERA5 wind fields
Tropopause definition	3 PVU; air parcels with PV ≥ 3 PVU were classified as being on the stratospheric side
Initial screening	Exactly one transition in PV classification within each consecutive, non-overlapping 1-h window
Residence-time criterion	Continuous retention of the original state before crossing and the destination state after crossing for 1, 2, 6, 12, or 24 h
Analysis domain used in the manuscript	Events selected according to crossing locations within 94-104°E and 25-32°N

Given the short-duration, rapid ozone-descent event examined in this study, the 1-h and 2-h criteria were used to implement the Lagrangian framework by identifying trajectory crossings, PV-state transitions, and subsequent residence-time persistence. These criteria were not intended to represent statistics of deep stratosphere–troposphere exchange.

Air parcels were released throughout the full ERA5 source domain, rather than only within the smaller analysis domain used in the manuscript. The manuscript domain was applied solely as a spatial filter based on the locations at which the crossings occurred. Consequently, parcels originating outside the analysis domain could be transported into it before undergoing a diagnosed crossing.

Increasing the number of released parcels improves the sampling density. However, it does not convert grid cells without physically diagnosed crossings into a spatially continuous field with nonzero values.

3.2 Residence-time sensitivity of the mass flux

Stay (h)	**STT events**	**TST events**	**STT mass (10^{12} kg)**	**TST mass (10^{12} kg)**	**Net downward mass (10^{12} kg)**	**Net upward mass (10^{-5} kg m^{-2} s^{-1})**
1	4,211	5,102	171.761	208.104	-36.343	-27.668
2	1,923	2,679	78.437	109.273	-30.836	-23.476
6	299	735	12.196	29.980	-17.784	-13.539
12	19	130	0.775	5.303	-4.528	-3.447
24	0	52	0.000	2.121	-2.121	-1.615

Under all five residence-time thresholds, the signed net downward flux is negative, indicating that troposphere-to-stratosphere transport (TST) dominates the 48-h total mass budget within the analysis domain under the present event definition. As the residence-time threshold increases from 1 to 24 h, both the number of diagnosed events and the absolute magnitude of the flux decrease monotonically. This indicates that the results obtained using short residence times include a substantial number of brief recrossings near the tropopause. Residence times of 6-24 h are therefore more appropriate for discussing relatively robust exchange, whereas the 1-h and 2-h thresholds should be treated as short-term sensitivity bounds.

4 Four-dimensional collocation with ERA5 ozone

For the 261,800 unique physical crossing points, ERA5 O_3 was interpolated in four dimensions using the crossing time, longitude, latitude, and pressure. The ozone mass mixing ratio ranged from 4.816×10^{-8} to 3.218×10^{-6} kg kg^{-1}, with a median of 1.814×10^{-7} kg kg^{-1}, corresponding to approximately 109.5 ppbv.

Stay(h)	Events	STT O_3 (10^6 kg)	TST O_3 (10^6 kg)	Downward O_3 (10^6 kg)	O_3 flux (10^{-11} kg m^{-2} s^{-1})	STT qO_3 (10^{-9})	TST qO (10^{-9})
1	9,313	39.623	46.316	-6.693	-5.095	230.69	222.56
2	4,602	16.676	22.436	-5.760	-4.385	212.61	205.32
6	1,034	2.502	5.704	-3.202	-2.438	205.12	190.26
12	149	0.242	1.134	-0.891	-0.679	312.77	213.80
24	52	0.000	0.421	-0.421	-0.321	NaN	198.57

Under all five residence-time thresholds, the regional net ozone flux is also negative, indicating that the total ozone mass transported by TST exceeds that transported by STT. This result remains consistent with the short-lived downward intrusion of ozone-rich air observed by the lidar at the fixed site. The site-specific downward intrusion and the regional 48-h net cross-tropopause ozone budget represent distinct diagnostic quantities with different spatial and temporal scales.

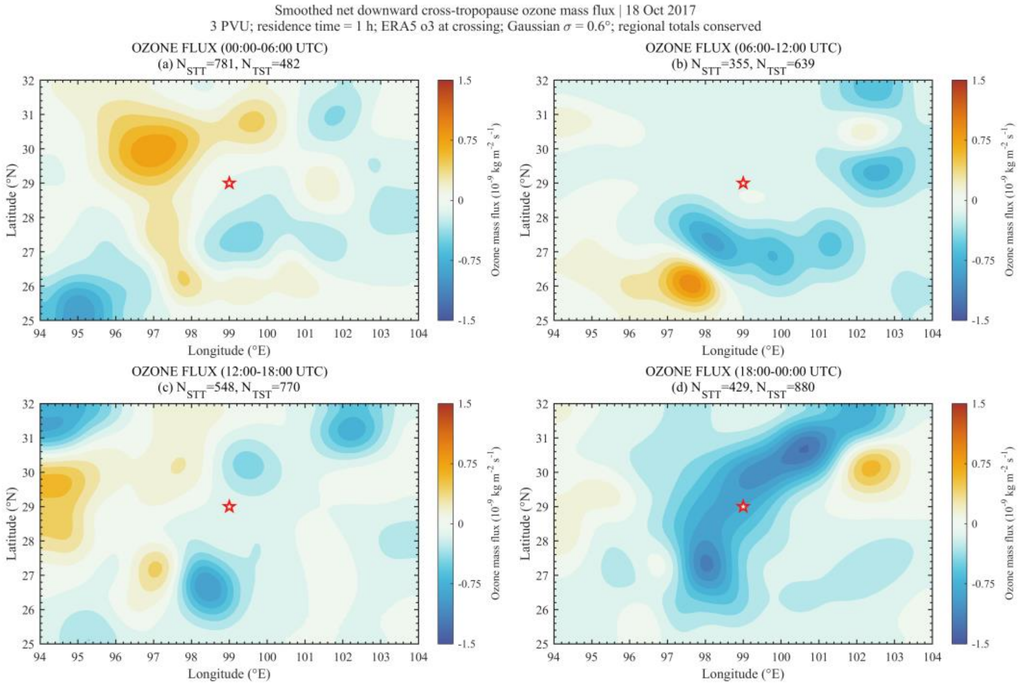

Fig.5. Six-hourly net downward ozone mass flux on 18 October 2017 after collocation with ERA5 ozone under the 1-h residence-time criterion.

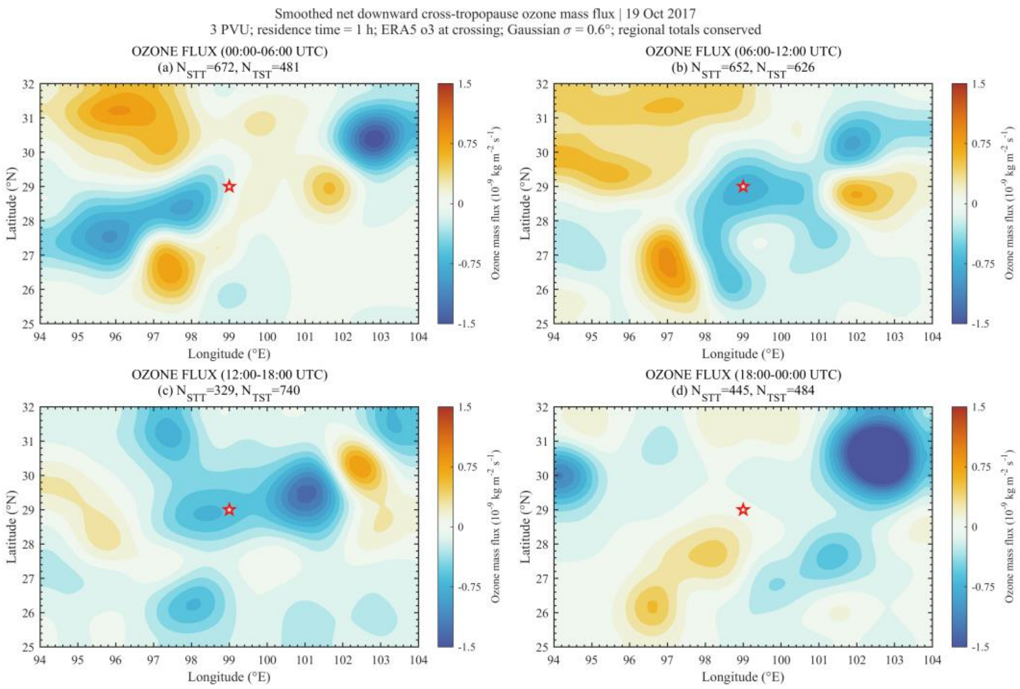

Fig.6. Six-hourly net downward ozone mass flux on 19 October 2017 after collocation with ERA5 ozone under the 1-h residence-time criterion.

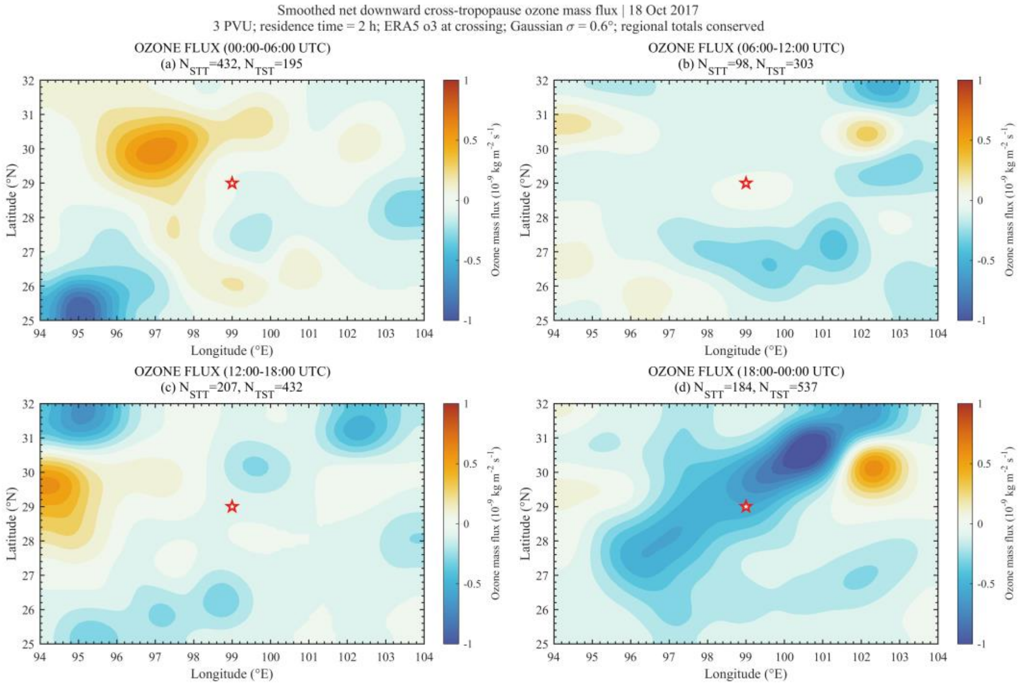

Fig.7. Six-hourly net downward ozone mass flux on 18 October 2017 after collocation with ERA5 ozone under the 2-h residence-time criterion.

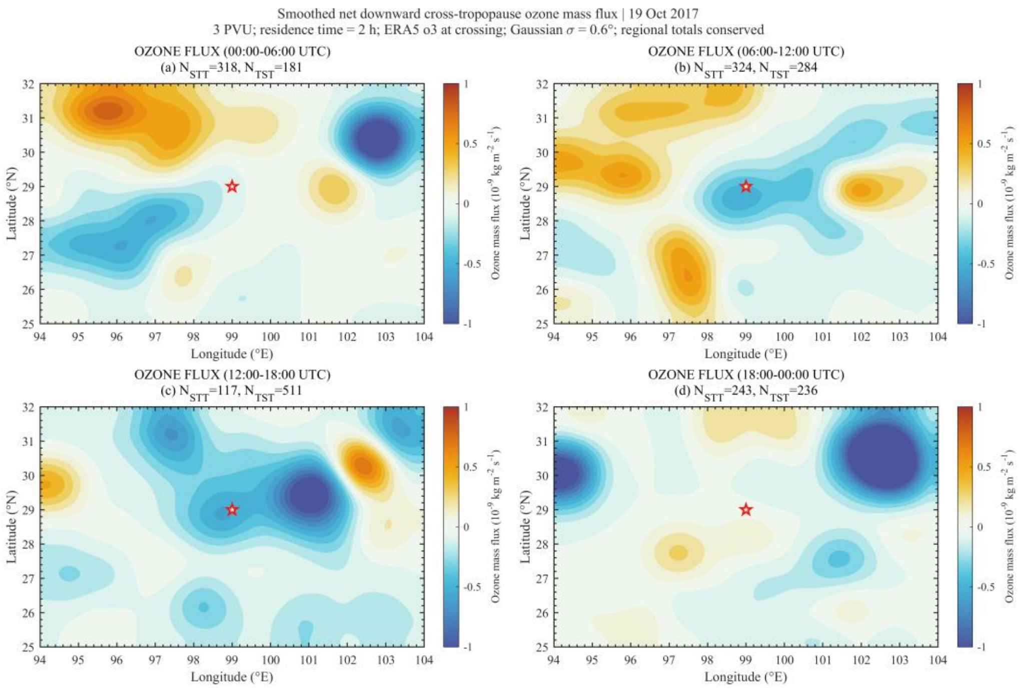

Fig.8. Six-hourly net downward ozone mass flux on 19 October 2017 after collocation with ERA5 ozone under the 2-h residence-time criterion.

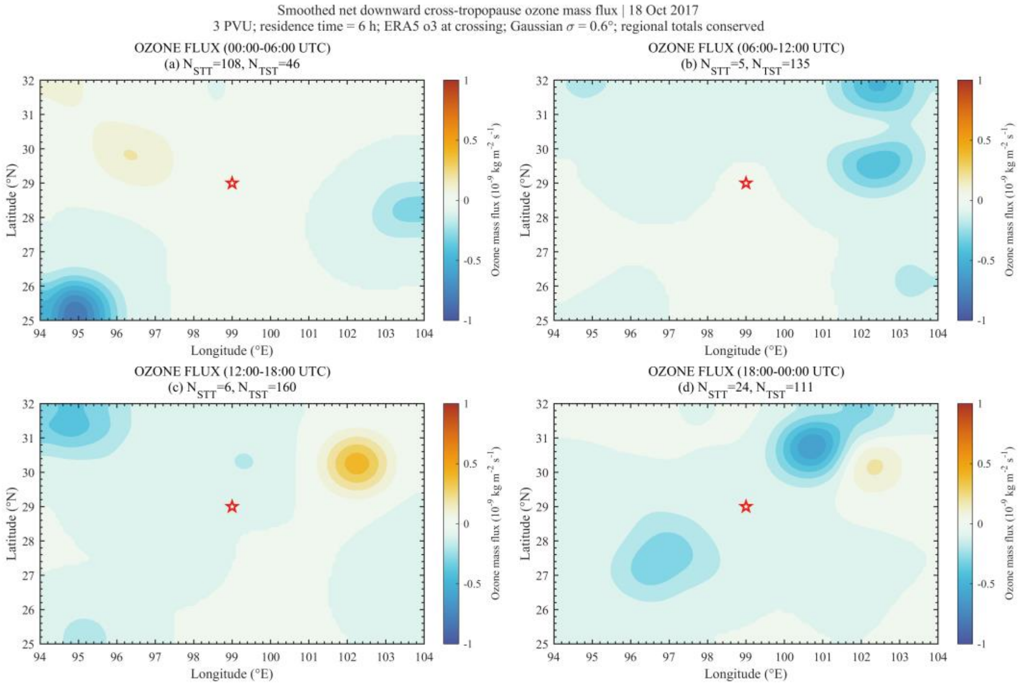

Fig.9. Six-hourly net downward ozone mass flux on 18 October 2017 after collocation with ERA5 ozone under the 6-h residence-time criterion.

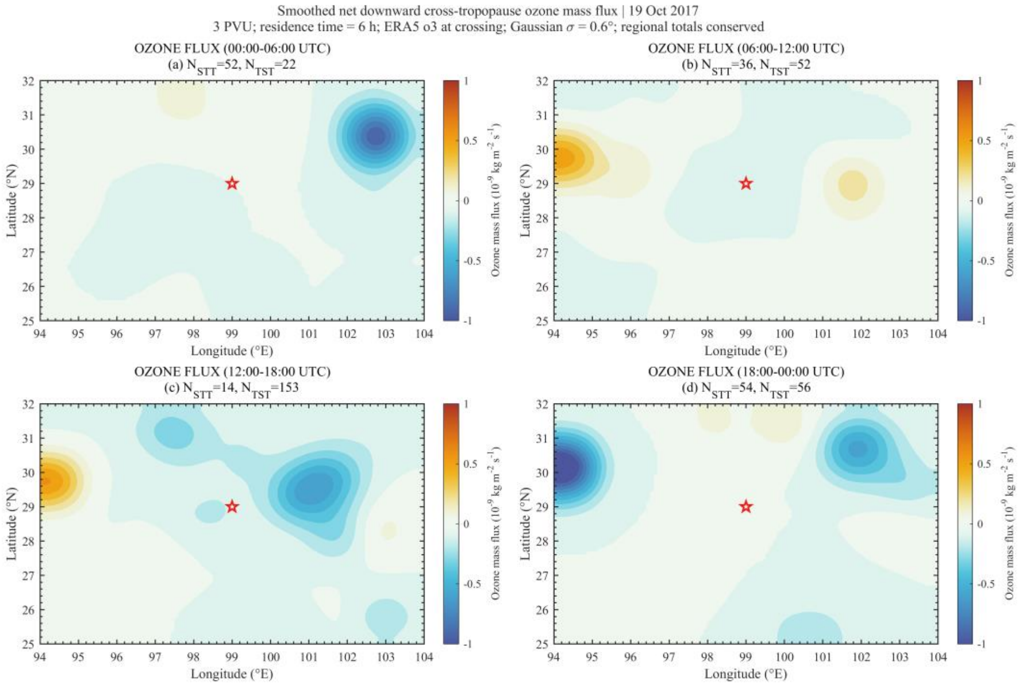

Fig.10. Six-hourly net downward ozone mass flux on 19 October 2017 after collocation with ERA5 ozone under the 6-h residence-time criterion.

5 Methodological comparison

Method	Criterion or Control Surface	Primary Output	Key Limitations
Wei's method in isobaric coordinates	Instantaneous Eulerian derivatives and a moving tropopause	Continuous full-coverage field; decomposition into three terms	Cancellation among large terms, numerical noise, and sensitivity to derivatives of the tropopause surface
Wei's method in potential vorticity coordinates	$(\partial p/\partial Q)(DQ/Dt)$ evaluated on the 3-PVU surface	Continuous field in PV coordinates; includes an internal consistency check	Remains within the Wei diagnostic framework; sensitive to multiple tropopauses and nonconservative PV evolution
Trajectory method with residence-time filtering	Air parcels cross the 3-PVU surface and remain on each side for a prescribed residence time	Traceable event mass, direction, location, and timing	Dependent on trajectory accuracy, parcel-release density, temporal resolution, and boundary treatment

5.1 Commonalities and differences

The principal commonality among the three diagnostics is qualitative. All three indicate pronounced spatiotemporal heterogeneity and bidirectional exchange near the 3-PVU surface during 18-19 October. Significant signals repeatedly occurred near 26-28°N and 97-99°E, supporting the association of this region with tropopause folding and related dynamical disturbances.

The differences are primarily quantitative and morphological. The continuous Wei fields produce alternating positive and negative structures across the entire domain. By contrast, the trajectory-based fields contain mass only at crossing locations that satisfy the prescribed screening criteria. Even after mass-conserving spatial smoothing, the resulting distributions remain confined to a limited number of event clusters. The trajectory analysis shows that TST dominates the 48-h total budget during most periods and under all residence-time thresholds. Therefore, neither the warm-colored area nor the peak values in Figs. 9-10 of the original manuscript can be used directly to infer a regional net STT budget.

This discrepancy does not imply that the lidar observations are incorrect. The lidar records local, short-lived, and high-resolution downward transport of ozone-rich air above Yangbajing, whereas the Lagrangian budget quantifies the total mass associated with bidirectional crossings that satisfy the residence-time criterion over the entire analysis domain during the 48-h period. Local STT and a regional net TST budget can

therefore occur simultaneously.
The current results provide high-confidence support for the occurrence of short-lived ozone descent near Yangbajing, active dynamical structures near the 3-PVU surface, and strong temporal variability and spatial heterogeneity during the event. The region spanning approximately 26-28°N and 95-99°E represents an important disturbance and tropopause-folding area, but this interpretation should be presented jointly with the PV cross-sections and trajectory analysis.

6 Proposed revisions and interpretation

The three sets of results consistently support the conclusion that the Yangbajing event occurred within a strongly disturbed, bidirectional, and spatially heterogeneous tropopause environment. I therefore suggest retaining Fig. 9, but limiting its interpretation to the relative spatial structures of the individual terms rather than using their absolute magnitudes as evidence of the mass associated with actual cross-tropopause transport. Alternatively, it could be replaced by the mass-flux results obtained in potential vorticity coordinates.
My current understanding and application of the Lagrangian method may still be limited. The results obtained with this method show considerable sensitivity to the prescribed residence time. In particular, the six relevant studies you provided applied residence-time criteria of 12 or 24 h when investigating global-scale deep stratosphere–troposphere exchange. The present study, however, focuses on the relationship between the short-duration, rapid downward-transport event observed by the lidar and other dynamical processes, including temperature disturbances. With your guidance, the Lagrangian method could be more closely integrated with the lidar observations to provide further analyses and independent validation of the observed event.

Appendix: Air parcels

1h residence time:

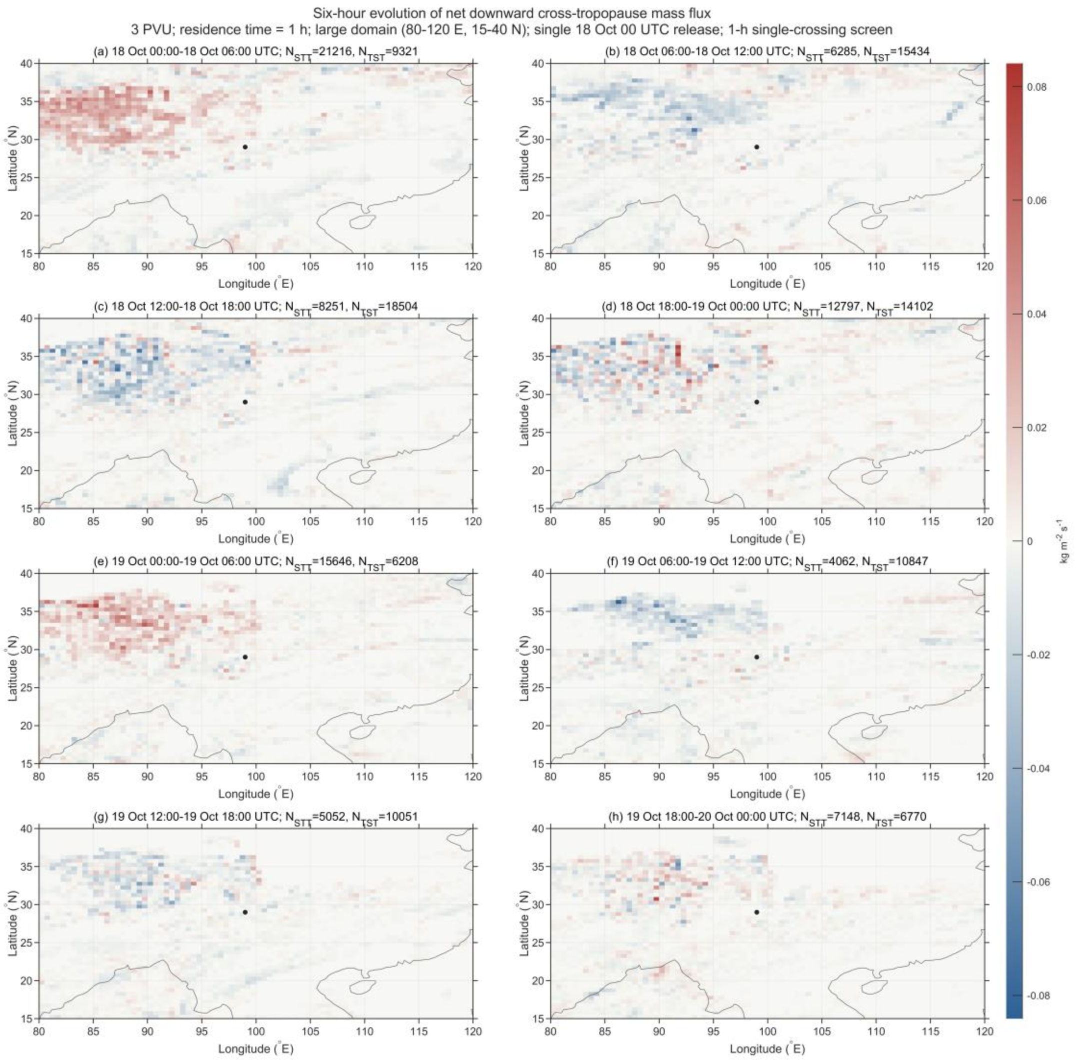

2h residence time:

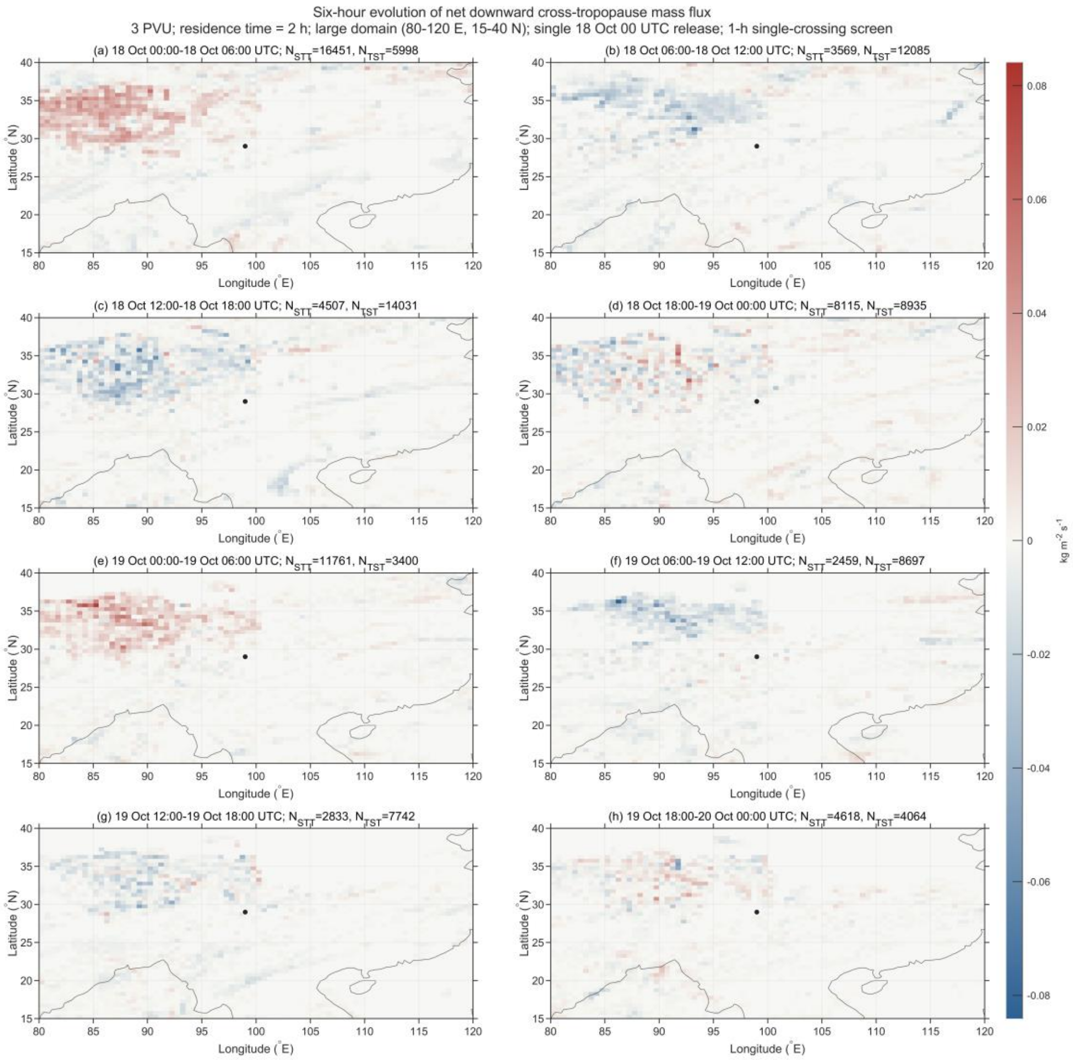

6h residence time:

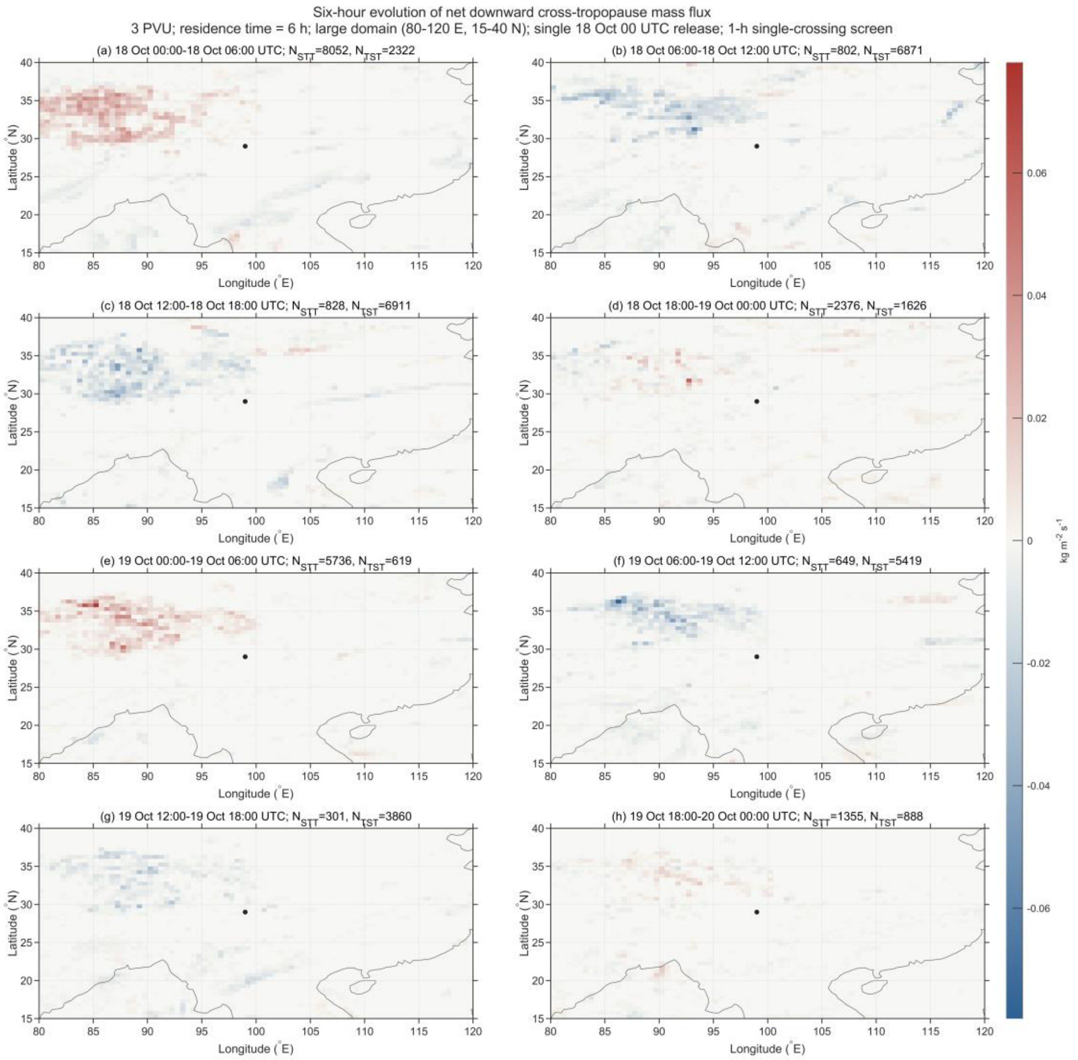

12h residence time: